Sensors and Materials, Vol. 34, No. 11 (2022) 4185–4208
MYU Tokyo

S & M 3105

Optical-fiber-type Contact Force Detector for Improving Safety and Workability of Myocardial Biopsy

Tomoyuki Umemoto,[1†] Kei Sato,[2†] Tetsuro Miyazaki,[3†*] Toshihiro Kawase,[4] Maina Sogabe,[3] Tetsuo Sasano,[1] and Kenji Kawashima[3]

[1]Department of Cardiovascular Medicine, Tokyo Medical and Dental University, 1-5-45 Yushima, Bunkyo-ku, Tokyo 113-8510, Japan
[2]Institute of Biomaterials and Bioengineering, Tokyo Medical and Dental University, 2-3-10 Kanda Surugadai, Chiyoda-ku, Tokyo 101-0062, Japan
[3]Department of Information Physics and Computing, The University of Tokyo, 7-3-1 Hongo, Bunkyo-ku, Tokyo 113-8656, Japan
[4]School of Engineering, Department of Information and Communication Engineering, Tokyo Denki University, Senju Asahi-cho, Adachi-ku, Tokyo 120-8551, Japan

(Received July 29, 2022; accepted October 19, 2022)

Keywords: myocardial biopsy, biopsy forceps, contact force detection, optical fiber, light intensity modulation

In a myocardial biopsy, the physician inserts the myocardial biopsy forceps into the heart chamber with fluoroscopic guidance and operates the forceps to collect the myocardium. The tip of the forceps has a gripper and a two-degree-of-freedom passive joint. The myocardial wall is difficult to see through a fluoroscopic image, and sampling may be missed due to the weak contact force and the large angle between the forceps and the myocardium. To solve these problems, we propose a contact force and bending angle detection mechanism for the forceps using optical fibers. The proposed mechanism has three built-in optical fibers and is connected to light-intensity-modulation-type optical sensors. Before contact, the light of the fibers leaks outside through the forceps shaft gap. When the forceps tip comes into contact with the myocardial wall, the external force reduces the shaft gap and the leak light amount. The physician can detect the contact force and bending state at the tip from the ratio of the three measured values. We evaluated the proposed mechanism in *in vitro* and *in vivo* experiments. We confirmed that the contact force under 1.4 N and bending angle over 30 deg can be detected.

1. Introduction

1.1 Background

The myocardial biopsy shown in Fig. 1 is a pathological examination performed when cardiomyopathy or myocarditis is suspected or after cardiac transplantation in order to monitor for allograft rejection. A physician performs this examination by sampling cardiomyocytes with myocardial biopsy forceps. Figure 2 shows an example of myocardial biopsy forceps, and Fig. 3

*Corresponding author: e-mail: Tetsuro_Miyazaki@ipc.i.u-tokyo.ac.jp
†These authors contributed equally to this work.
https://doi.org/10.18494/SAM4049

ISSN 0914-4935
https://myukk.org/

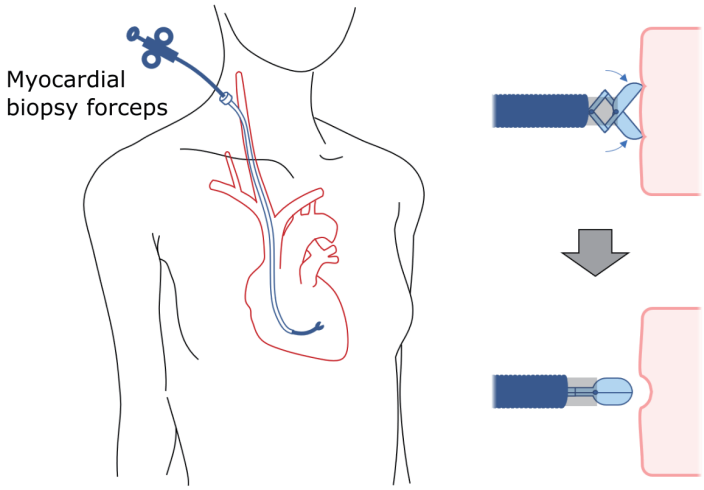

Fig. 1. (Color online) Myocardial biopsy.

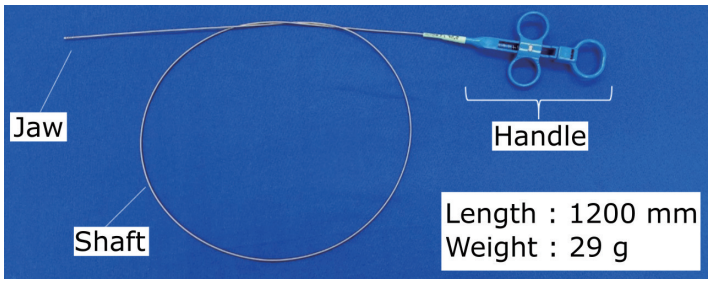

Fig. 2. (Color online) Example of myocardial biopsy forceps.

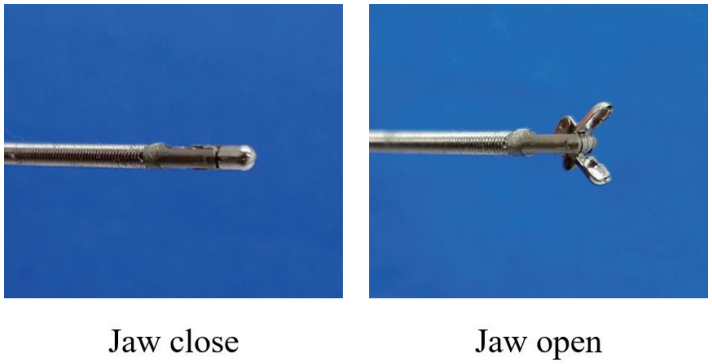

Fig. 3. (Color online) Myocardial biopsy forceps jaw.

shows an enlarged view of the tip of the forceps. Myocardial biopsy forceps have been used unchanged since the original was developed by Sakakibara and Konno in 1962.[1,2] The forceps have a mechanism with a gripper part called a jaw attached to the tip of a bendable shaft. We assumed that the forceps tip has a two-degrees-of-freedom passive rotary joint since the bendable shaft is a continuous flexible metal coil spring. The physician can open and close the jaw by operating the handle. For the myocardial biopsy, the physician manipulates the forceps

with fluoroscopy guidance. However, the myocardial wall is difficult to recognize with the fluoroscopic device, and the contact response between the forceps and the myocardium is very weak. Therefore, it is difficult to determine the contact state visually and tactilely. Such blind work may cause serious complications,[3–6] including pericardial fluid retention and cardiac tamponade by perforation of the myocardial wall, which can be lethal. In addition, sampling miss, that is, the physician withdraws the forceps without sufficient contact between the jaw and the myocardial wall, will also occur. These problems are caused by the fact that the contact judgment between the jaw and the myocardial wall depends on the subjectivity of each physician, and it is difficult to judge the contact state objectively and quantitatively. While much interest has been placed in the diagnosis of cells collected by biopsy,[6,7] there are few cases in which the mechanism of the myocardial biopsy forceps itself has been improved and novel functions have been added.

Moreover, in recent medical treatment, percutaneous surgery with an emphasis on the patient's quality of life is required. In surgical care, minimally invasive surgery tends to be preferred. In the conventional surgical method, in order to reach the target site with surgical instruments, a large incision is made in the normal site to make the surgical space. On the other hand, minimally invasive surgery treats lesions while minimizing damage to normal tissue.[8,9] This method is adopted in many surgical fields[10–15] such as myocardial ablation, prostatectomy, cholecystectomy, cystectomy, hysterectomy, and nephrectomy, owing to the advantages of significantly reducing postoperative pain and shortening the recovery time of patients. Minimal invasiveness is also important in biopsy diagnosis, and the method of percutaneously collecting tissue is preferable to the method of collecting tissue by open surgery. The above-mentioned myocardial biopsy forceps is one of the percutaneous surgical instruments. However, long instruments such as the biopsy forceps contacts various sites along the vessel path before the forceps tip reaches the target site. The contact friction force in the vessel path becomes noise and impairs the force information of the small contact force at the forceps tip. For this reason, in myocardial biopsy tasks, it is difficult for physicians to accurately control the contact force of the forceps tip by the feel at hand. This issue leads to the prolongation of operating time and damage risk to the target site.

1.2 Conventional research

In recent years, research on haptics, robotics, and computer-integrated surgery has been actively conducted, and minimally invasive surgery has been considerably improved. Various force information technologies have been proposed to solve the problem of lack of force information in minimally invasive surgery.[16–18] For example, the force measurement range for robotic forceps grippers is 0.5 to 10 N. The force measurement range with a catheter insertion robot, such as for ablation, is generally 0 to 0.5 N. In addition, sensor-integrated tools have been designed, such as force-sensing forceps,[19,20] force-controlled grippers,[17,21,22] and sensor-integrated scalpels.[23,24] For example, Tanimoto *et al.*[25] proposed a small-diameter force sensor using strain gauges for a catheter surgery robot. This sensor has a diameter of 1.2 mm, a length of 5 mm, and a resolution of 0.5 mN.

However, these devices have limited applicability to the myocardial biopsy forceps in terms of sensing ability, accuracy, cost, size, and disposability.[16] In general, the myocardial biopsy forceps is disposable and has a small diameter; therefore, a small and low-cost sensor is required. Conventional force sensors include strain gauges and load cells that are commercially available for robots and industrial use. However, these are generally expensive,[18] difficult to sterilize, and difficult to apply to the myocardial biopsy forceps.

On the other hand, as a powerful solution to be installed in medical equipment, the force detection method using optical fiber sensors in medical devices has been actively researched.[26] In principle, measurement using light is robust from electrical noise. In addition, the optical fiber sensor has a simple mechanism, excellent corrosion resistance, and biocompatibility, and it is lightweight and inexpensive. In medical devices where safety is important, the simplicity of the structure is essential for reducing the risk of failure. Similarly, it is advantageous in terms of safety that no current flows through the part to be inserted into the body. In addition, a low manufacturing cost is required for the myocardial biopsy forceps, which is basically disposable after one-time use in order to prevent infection. Thanks to these merits, force sensors using optical fiber sensors have been developed.

Fiber optic sensors are broadly classified according to three measurement principles: light intensity modulation (LIM),[27–39] fiber Bragg grating (FBG),[40–45] and Fabry–Perot interferometry (FPI).[46–53] The advantages and disadvantages of each measurement principle are as follows. First, the advantages of LIM sensors are that the sensor has a cheap and simple structure and is less affected by temperature change. The disadvantages are that the LIM sensor is sensitive to fluctuation in the light source and misalignment between component parts, and the measured value sometimes gets drift noise. Second, the advantages of FBG sensors are that the sensor can measure small microscale strain and is sterilizable. The disadvantage is that the signal processing system requires a relatively expensive light source and optical interrogator. In addition, the FBG sensor is temperature-sensitive and needs compensation. Finally, the advantages of FPI sensors are that the measurement range can be adjusted, they have high sensitivity, signal processing is relatively simple compared with the FBG sensor, and the FPI sensor can be sterilized. The disadvantages are that the assembly accuracy is important for the FPI sensor and the manufacturing difficulty is high. Also, the FPI sensor has a cavity inside, so it is easily damaged, and the sterilization process tends to be complicated.

As examples of LIM sensors, Yip *et al.*[30] proposed a compact uniaxial force sensor for use in the beating heart during mitral annuloplasty. The diameter of the sensor is 5.5 mm and the length is 12 mm. The deformation of the soft elastomer component is measured from the reflected light intensity, and force of 0 to 4 N can be measured with a root mean square error of 0.13 N. However, since this sensor has a closed structure attached to the tip of the instrument, it is difficult to apply it to myocardial biopsy forceps with a jaw at the tip of the instrument. Puangmali *et al.*[31] proposed a three-axis LIM-type force sensor for palpation. The sensor can measure axial force of ±3 N and radial force of ±1.5 N with its resolution of 0.02 N. However, the unique monolithic flexible tripod part is a complex-shaped component that is as large as 10 mm in diameter, and it is difficult to attach to the myocardial biopsy forceps with a diameter of approximately 2 mm.

As an example of FBG sensors, Yokoyama *et al.*[41] proposed a three-axis force sensor for an open-irrigated radiofrequency (RF) ablation catheter. The sensor diameter was 3.5 mm, the measurement range was 0 to 0.5 N, and the resolution was 10 mN. However, the FBG sensor is more expensive than the LIM-type sensor.

As an example of FPI sensors, Liu *et al.*[51] mounted a miniature needle-type force sensor with an outer diameter of less than 1 mm on a vitreous retinal surgical instrument. The maximum force of 6 mN can be measured with its resolution of 0.25 mN. However, FPI sensors are also expensive and difficult to mount on disposable biopsy forceps.

On the basis of the above three measurement principles, we considered a method suitable for mounting the sensor on myocardial biopsy forceps. The wire for manipulating the open and closed positions of the jaw is located at the center of the myocardial biopsy forceps. Therefore, to realize small-diameter forceps, it is rational to place multiple thin sensors on the outer circumference instead of placing one thick sensor in the center of the forceps. The LIM-type sensor's diameter is easy to reduce, and it is advantageous for miniaturization. In addition, LIM fiber components are inexpensive and can maintain the disposableness of the forceps.

1.3 Contribution of this research

Considering the issues mentioned above, in this study, we propose a novel contact force and bending angle detection mechanism using LIM-type optical fiber sensors for the myocardial biopsy forceps. The proposed detection mechanism utilizes the structure of the myocardial biopsy forceps and mounts small-diameter and disposable optical fibers on the forceps. Thanks to the explicit and quantitative detection, the proposed detection mechanism can be used to carry out the biopsy task while ensuring safety, and we evaluated its clinical usefulness. The proposed mechanism will prevent problems such as trial miss and fatal damage and reduce the physician's effort (number of trials) and incident risk (complications). The proposed mechanism incorporates inexpensive optical fibers in the forceps and connects the fibers to the light intensity sensors outside the patient's body. With this configuration, it is possible to detect the contact force and bending angle at the forceps tip while maintaining the disposability of the forceps part.

This paper is organized as follows. In Sect. 2, we describe the proposed mechanism and experimental setups for evaluating the performance of the proposed mechanism. In Sect. 3, we describe the experimental results. In Sect. 4, we discuss the results, and finally, in Sect. 5, we draw the conclusions.

2. Method

2.1 Measurement principle of proposed mechanism

2.1.1 Deformation of myocardial biopsy forceps

In this paper, we propose a force sensing method that utilizes the deformation of the shaft due to the opening and closing of the jaw of the myocardial biopsy forceps. Figure 4 shows a

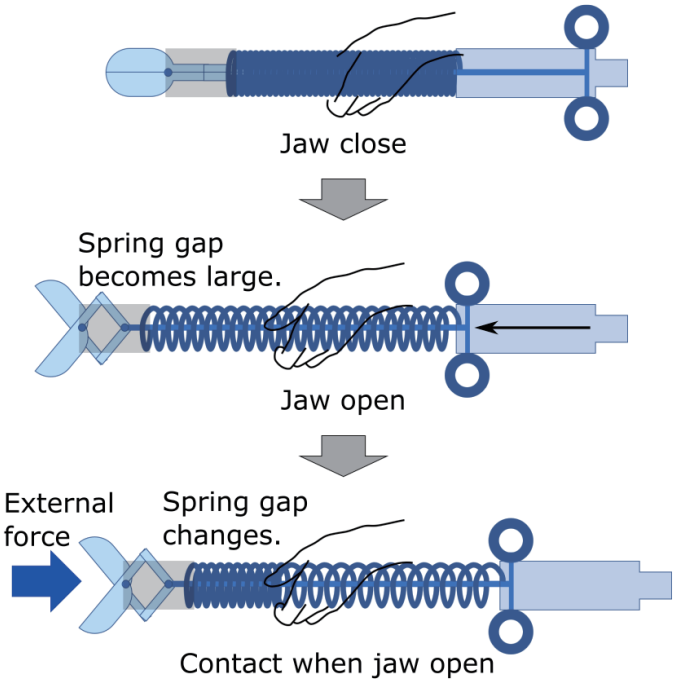

Fig. 4. (Color online) Deformation of shaft of myocardial biopsy forceps.

schematic diagram of the shaft deformation. In actual surgery, it is necessary to detect the contact force when the forceps tip comes into contact with the myocardium in a jaw-open state. The jaw opens by manipulating the handle and pushing in the wire connected to the jaw's linkage. Theoretically, the pushing depth required to open and close the link mechanism is about 1 mm, but in reality, it is necessary to push the handle about 10 mm since the shaft spring is extended by the pushing force. The distortion caused by pushing the wire excessively is eliminated by extending the close-contact spring-type shaft. In other words, there is a gap in the shaft when the jaw opens in contact with the myocardial wall. Finally, when the jaw gets external force by coming into contact with the heart wall, the spring gap near the forceps tip will change. We considered utilizing the gap change for the contact state detection.

2.1.2 Concept of proposed detection mechanism

We propose a mechanism that can detect external force in any direction applied on the tip by incorporating three pairs of LIM-type optical fiber sensors and a conical reflector. Figure 5 shows a cross-sectional view of the proposed forceps model prototype. The optical fibers are built in the shaft of the forceps model, and the end face of the fiber that goes out of the patient's body is connected to the LIM sensor. The conical reflector is placed near the tip of the forceps model and faces the ends of the optical fibers. This is the first development trial of the proposed concept in this study, and we focused on realizing the contact detection function; therefore, we manufactured a simple forceps model without the jaw and wire. To simulate the gap of the shaft, a part near the tip of the close contact coil spring was plastically deformed and processed into a compression spring, and this was used as a shaft model. One optical fiber sensor consists of two

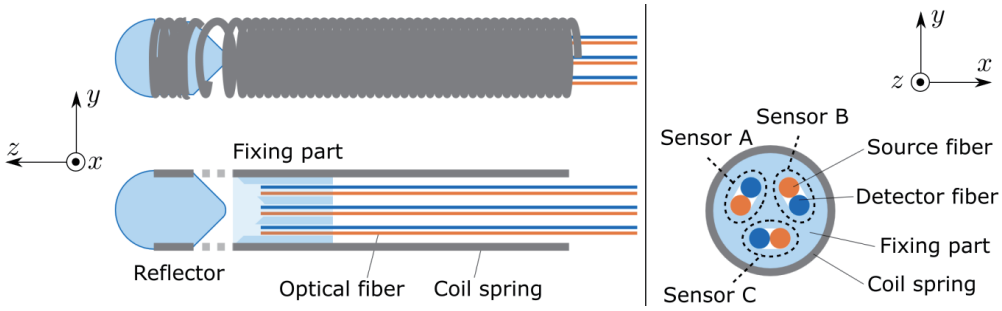

Fig. 5. (Color online) Cross-sectional view of proposed forceps model prototype.

fibers, a light source fiber (orange) and a light detector fiber (blue), and the three sensors are arranged to form an equilateral triangle on the radial cross section using the fixing part as shown in Fig. 5. The three sensors are distinguished as A, B, and C. Thanks to this configuration, the three-dimensional bending angles of the forceps tip rotating on the *xz* and *yz* planes can be measured by the three sensors. The fixing part was fixed to the tip of the close contact coil spring part and faces the conical reflector. The rear end of the reflector has a hemispherical shape to prevent damage to the contact object due to the spring cross section at the tip of the shaft.

Figure 6 shows the assumed contact states and the targeted detection information. We aim to detect the external pushing force and bending angle of the forceps tip. By using the information, we can distinguish the three contact states, namely, no contact, appropriate contact, and bad contact. The no contact state should be detected to decrease the number of sampling misses. In the appropriate contact state, the pushing force is suitable for a safe and stable sampling task, and the forceps tip does not bend. When the forceps tip has a large bending, the sampling may fail, and this state should also be avoided.

Figure 7 shows a conceptual diagram of the external pushing force detection. When there is a gap in the shaft in a no contact state, the light reflected in the radial direction of the shaft leaks to the outside through the gap. After the jaw contacts the myocardial wall, the gap in the shaft shrinks due to external force, and the amount of light leakage decreases. By changing the amount of light, the contact force at the tip can be detected continuously.

Figure 8 shows a conceptual diagram of the bending angle detection. When the tip of the forceps bends due to contact, the size of the gap in the shaft differs between the inside and outside of the bend. When there is only one optical fiber built into the forceps, it bends as a result of contact, but there are cases where contact cannot be detected, such as when the gap near the optical fiber after bending is the same as the gap not in contact. Therefore, by arranging three pairs of optical fiber sensors isotropically, the measured value of either sensor changes regardless of the bending direction, and contact detection is possible. Furthermore, as shown in Fig. 8, the conical reflector is effective for detecting the bending state. By using the conical reflector, the amount of reflected light increases in the inner fiber and decreases in the outer fiber with respect to bending. This causes the difference in the amount of light for each channel, and the bending posture can be detected.

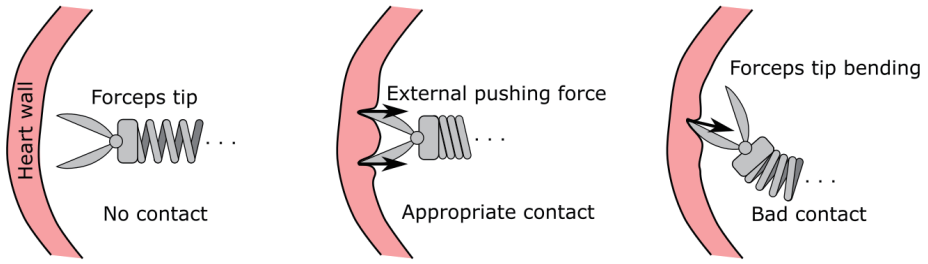

Fig. 6. (Color online) Three contact states and the targeted detection information.

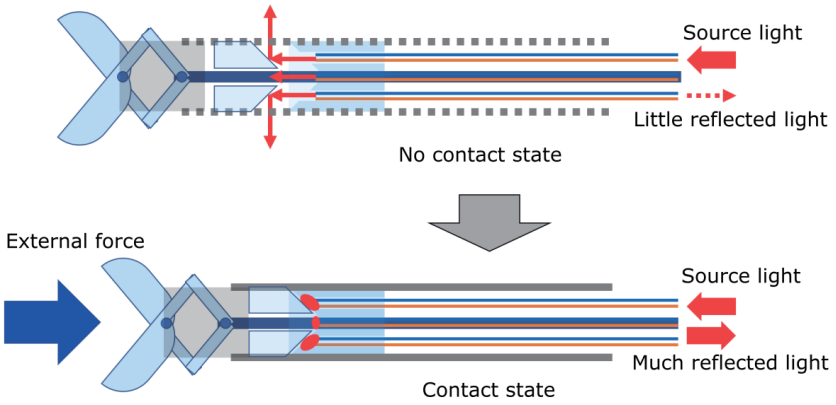

Fig. 7. (Color online) External pushing force detection.

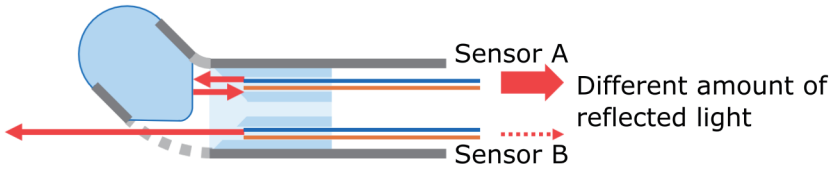

Fig. 8. (Color online) Bending angle detection.

Although the proposed mechanism can continuously measure the vertical pushing force and bending displacement, it is difficult to maintain a constant pushing force against the beating inner wall of the heart; therefore, in this study, we target the following binary mode judgment. The required specifications set as the contact judgment function are as follows.

(i) Binary judgment with and without contact is possible.

(ii) The mechanism can judge whether there is a large bend or not.

Specification (i) intends to prevent sampling miss and fatal complications, and specification (ii) intends to prevent certain bending conditions not suitable for sampling. Regarding specification (i), if the spring at the tip of the mechanism is not deformed without applying an external force, the measured value will be constant at 0% reflected light intensity. On the other hand, when an external force is applied and the spring at the tip of the mechanism is deformed, the measured value changes. In particular, when it is in contact with the inner wall of the heart, periodic changes in the measured value will be observed along with the pulsation, and we judge this state to be in contact. For specification (ii), a particular bend condition increases the likelihood that the jaw will not point towards the inner wall of the heart when the contact angle is large and myocardium sampling will fail. The sampling success rate will increase by judging the suitable contact states when the bending is sufficiently small. Specifically, if there is a change in all the measured values of the three sensors, we judge that a bending angle is small and a contact state is desirable. If there is no change with some of the three sensors, we judge that there is a large bending and a contact state will not be suitable for sampling.

2.2 External pushing force detection

We describe the power change of the reflected light using Fig. 9. To easily estimate the power change of the reflected light caused by the external pushing force in the z-axis direction, we consider the deformation of the coil spring shaft on the yz plane. In Refs. 28 and 29, the source light is modeled as a cone shape. In this model, the farther the light projection distance, the larger the irradiation area, and the light intensity per unit area is attenuated. On the other hand,

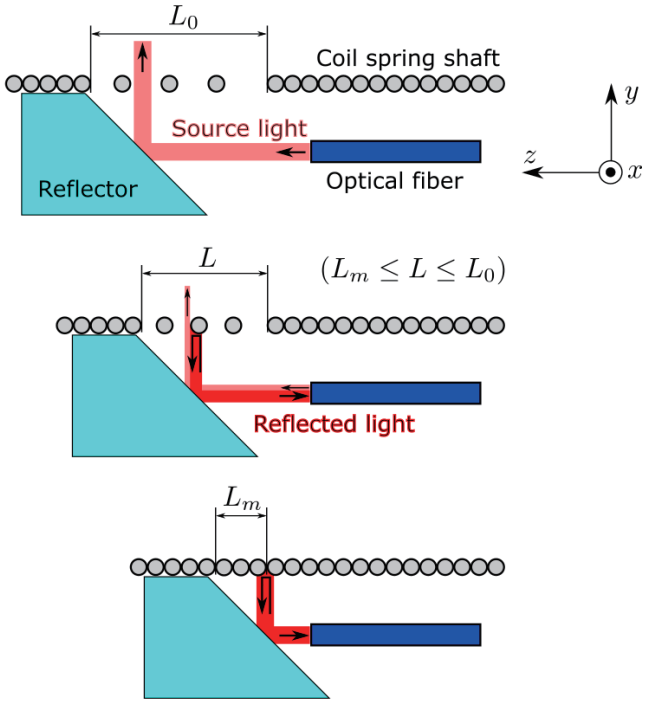

Fig. 9. (Color online) Enlarged view near the spring gap.

in our model shown in Fig. 9, we considered that the change in the reflected light power is dominated by the amount of spring gap rather than the projection distance. We assumed the source light to be cylindrical in shape whose diameter is constant in order to simplify the light power calculation. As shown in Fig. 9, the spring gap length is defined as L ($L_m \leq L \leq L_0$). L_0 is the initial gap, and L_m is the minimum gap length whose spring gap becomes almost 0. When the spring gap is L, the reflected light power P is assumed as

$$P(L) = P_S (L_m / L), \tag{1}$$

where P_S is the power of the source light. When L decreases, the spring gap decreases and the reflected light power increases monotonically. In Eq. (1), L_m / L corresponds to the ratio of the inner wall area of the spring shaft that reflects light to the projected area including the spring gap.

2.3 Bending posture detection

We describe the reflected light power of the conical reflector using Fig. 10. The vertex of the reflector is on the point z_0 of the z-axis at any bending angle. In the bending deformation of the forceps tip, it is necessary to consider the rotation of the reflector on the xz and yz planes around z_0. Although there are three built-in fibers, they are arranged point-symmetrically at intervals of 120 deg from the center of the shaft; therefore, analysis of one sensor can be applied to the other two sensors.

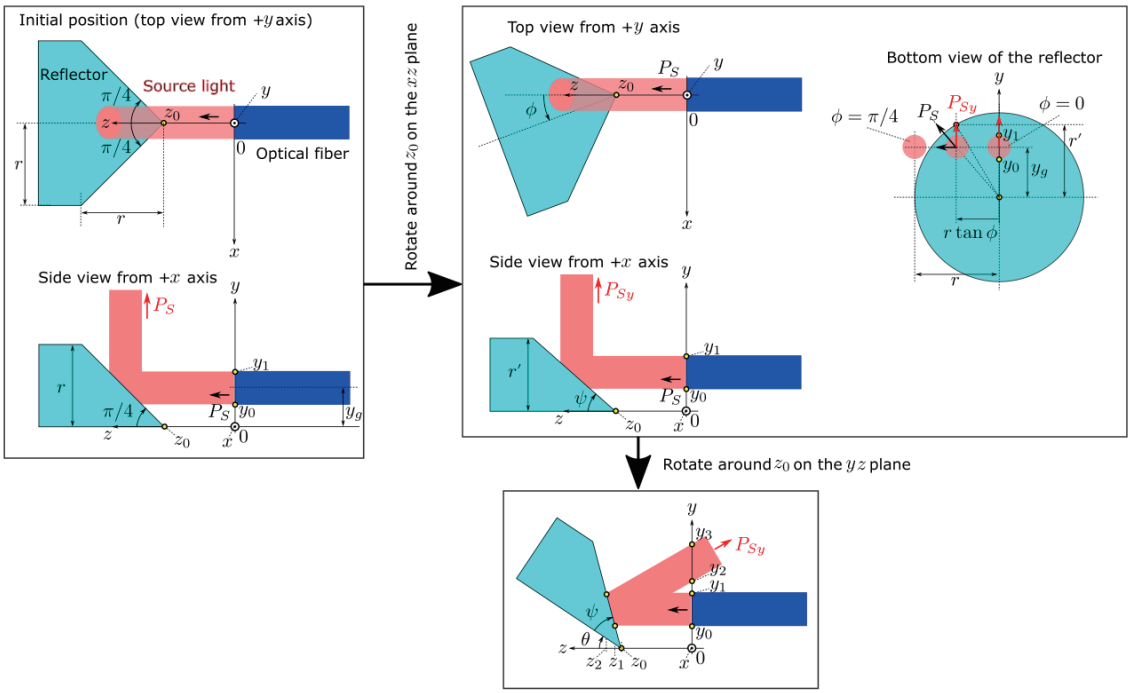

Fig. 10. (Color online) Enlarged view near the reflector when the forceps tip bend.

In the initial position, we assume that the central axis of the reflector and the optical fiber is on the *yz* plane, and the center of the optical fiber has offset y_g from the *z*-axis as shown in Fig. 10 (left).

First, we rotate the reflector by ϕ rad around z_0 on the *xz* plane from its initial position. The source light is reflected on the reflector surface and its *y*-component P_{Sy} is calculated as

$$P_{Sy}(\phi) = \begin{cases} \dfrac{y_g}{\sqrt{(r\tan\phi)^2 + {y_g}^2}} P_S. & \left(r^2 \geq {y_g}^2 + (r\tan\phi)^2\right) \\ 0. & \left(r^2 < {y_g}^2 + (r\tan\phi)^2\right) \end{cases} \tag{2}$$

In the case of $r^2 \geq {y_g}^2 + (r\tan\phi)^2$, the source light irradiates the reflector surface and the reflected light power P_{Sy} changes with the angle ϕ. In the case of $r^2 < {y_g}^2 + (r\tan\phi)^2$, the angle ϕ is too large, the source light will not irradiate the reflector, and P_{Sy} will become 0. In addition, the angle ψ of the reflector on the *yz* plane is also obtained as

$$\psi(\phi) = \tan^{-1}\sqrt{\frac{1-(\tan\phi)^2}{1+(\tan\phi)^2}}. \tag{3}$$

We use P_{Sy} and ψ in the following calculation.

Next, we rotate the reflector by θ rad around z_0 on the *yz* plane as shown in Fig. 10 (bottom). When the forceps tip bends with θ, the width of the source light is given from the fixed points y_0 and y_1, and the irradiation area of the reflected light on the *y*-axis is given from the variable points y_2 and y_3. When the bending angle is θ, the reflected light power P measured by the LIM sensor is assumed as

$$P(\phi,\theta) = \begin{cases} 0, & (y_1 < y_2) \\ P_{Sy}(\phi)\dfrac{y_1 - y_2}{y_3 - y_2}, & (y_2 \leq y_1 \leq y_3) \end{cases} \tag{4}$$

$$y_2 = y_0 + z_1\tan(\pi - 2\theta - 2\psi), \quad y_3 = y_1 + z_2\tan(\pi - 2\theta - 2\psi), \tag{5}$$

$$z_1 = z_0 + y_0\tan(\pi/2 - \theta - \psi), \quad z_2 = z_0 + y_1\tan(\pi/2 - \theta - \psi). \tag{6}$$

In the case of $y_1 < y_2$, the reflected light will not enter the optical fiber, and P will become 0. On the other hand, when the reflector bends and the condition of $y_2 \leq y_1 \leq y_3$ is satisfied, P increases along with θ. When $\theta + \psi = \pi/2$ and $y_1 = y_3$, P is maximized in each ϕ.

2.4 Manufacturing the prototype

We produced a prototype model of 3 mm diameter shown in Fig. 11 for detailed examination in *in vitro* and *in vivo* animal experiments. For the model, the fixing part and reflector were molded with a resin material using a stereolithography-type 3D printer (Formlabs, Form2), and metallic luster was given by a paint containing metal powder. An optical fiber of 0.5 mm diameter was used in this model. The optical fibers are connected to a fiber amplifier (Keyence, FU-N11MN) at the base of the forceps. The contact coil spring used for the shaft had a wire diameter of 0.3 mm and a diameter of 3 mm (Accurate, L008). The spring constant of the compression spring part was about 1.4 N/mm. In the force sensing of intracardiac surgery in conventional studies, the measurement is generally performed in the range of 0–0.5 N.[37,41,44,54,55] We considered that the myocardial biopsy task can be achieved if the contact force is similar to those in these studies, and we constructed the mechanism to sufficiently satisfy the measurement range of 0–0.5 N in this study as well.

2.5 *In vitro* experiments for performance evaluation

2.5.1 Change of light amount with respect to vertical external force

We carried out two *in vitro* experiments to confirm whether the proposed forceps prototype can detect any external force at the tip. As the first experiment, we evaluated the relationship between the vertical force and the amount of reflected light measured by the optical fiber sensor, and we confirmed whether the vertical external force can be detected.

Figure 12 shows a schematic diagram of the experimental setup. We fixed the prototype shaft on a desk and applied a force sensor (Imada, DS2-50n) perpendicular to its tip. We pushed the

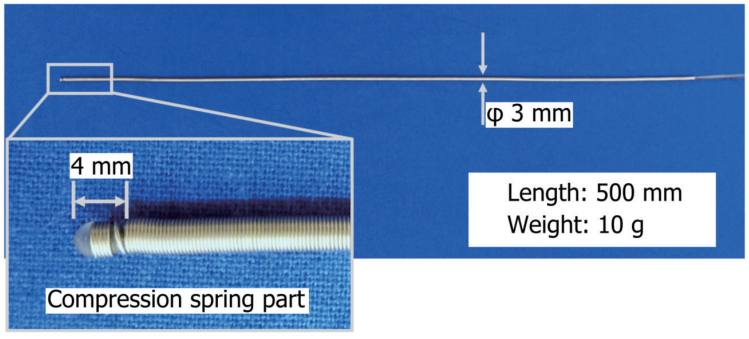

Fig. 11. (Color online) Proposed forceps model prototype (3 mm version).

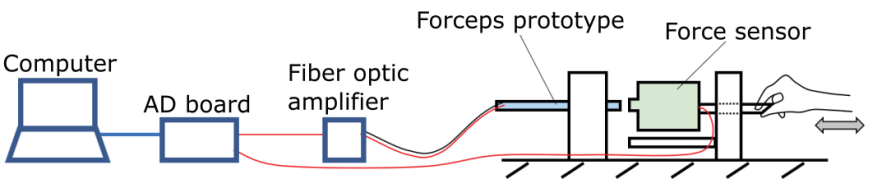

Fig. 12. (Color online) Experiment of vertical force detection.

forceps tip until the compression spring part was in close contact, and then we pulled the force sensor to its initial position. Three pairs of optical fibers are extended from the rear end of the prototype and connected to fiber optic amplifiers. The fiber optic amplifiers output the voltage converted from the amount of reflected light, and the voltage is input to an analog-to-digital (AD) board (National Instruments, NI-USB-6211). The measured voltage of the force sensor is also input to the AD board. These measured voltages were recorded on a computer at a sampling frequency of 100 Hz. The acquired data was filtered by a moving average filter in intervals of 10 steps to remove high-frequency white noise and thinned out in intervals of 10 steps to reduce the data number.

The measured values of the three sensors vary depending on the individual differences of the sensors and the assembly error of the mechanism. To compensate for these variations, we carried out the normalization shown in Fig. 13 as a calibration process that gives the relationship between the spring displacement and the sensor measured value. Specifically, we removed the offset of the raw data by subtracting the minimum value of each data, and we normalized the data by dividing each data range. The measured value in the initial state without deformation is set to 0% light intensity, and the measured value at the maximum displacement where the compression spring is completely compressed is set to 100% light intensity. The measured values are normalized for each sensor. For vertical pushing, the amount of deformation and the force of the compression spring have a linear relationship; therefore, we can obtain the amount of deformation and the generated force from the measured values of the normalized sensor.

2.5.2 Change of light amount with respect to bending angle

In the second experiment confirming the change of the light amount with respect to the bending angle, we measured the amount of reflected light when the forceps tip was pushed laterally and bent. We confirmed the bending detection performance of the conical reflector.

Figure 14 shows a schematic of the experimental setup. We fixed the prototype shaft on the desk and bent its tip by using a rotating jig shown in Fig. 15. After inserting the tip of the prototype into the hollow section of part B, the tip was bent by inserting part A into the through-hole opened in part B. We made three types of jig with the tip bending angles of 15, 30, and 45 deg.

As shown in Fig. 14, we rotated the jig around the axis of the prototype with its tip inserted in the jig. The tip changed its bending direction while sliding on the outer wall of the hollow hole of

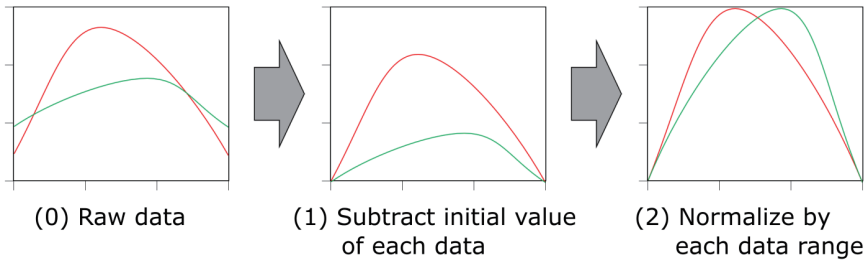

Fig. 13. (Color online) Sensor calibration process.

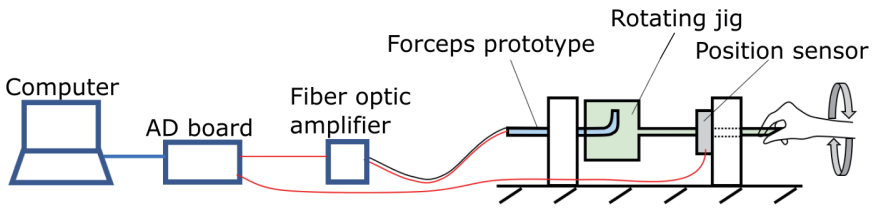

Fig. 14. (Color online) Experiment of bending angle detection.

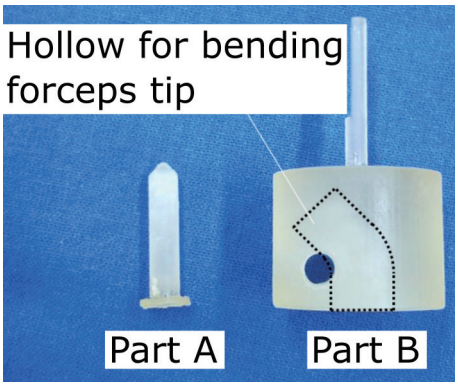

Fig. 15. (Color online) Rotating jig.

the jig. The jig is mechanically connected to the rotational position sensor (ALPS ALPINE, RDC501051A), and the output of the position sensor changes according to the rotation angle of the jig. The measured voltages of the optical fiber sensors and position sensor were input to the AD board and recorded on the computer at a sampling frequency of 100 Hz. The acquired data was filtered by a moving average filter in intervals of 10 steps to remove high-frequency white noise and thinned out in intervals of 10 steps to reduce the data number. We used the same data calibration process described in the previous section.

2.6 Animal experiment using live pig

To confirm the feasibility of the proposed contact state detection in an actual *in vivo* surgical environment, we carried out an animal experiment using a live pig. Figure 16 shows the scenery and setup of the animal experiment. The prototype's diameter of 3 mm is almost the same as the real myocardial biopsy forceps' diameter of about 2 mm. The configuration from the three pairs of optical fiber sensors to the AD board was the same as in the previous section. In this experiment, the measured voltage of the electrocardiograph was also input to the AD board. A moving average filter in intervals of 50 steps was applied to the data acquired at a sampling frequency of 1000 Hz to remove high-frequency white noise. A cardiologist who performs myocardial biopsy as a daily task operated the forceps prototype and traced the actual biopsy procedure in this experiment. The physician pushed the tip of the prototype against the myocardial wall and observed whether changes would occur in the measured data.

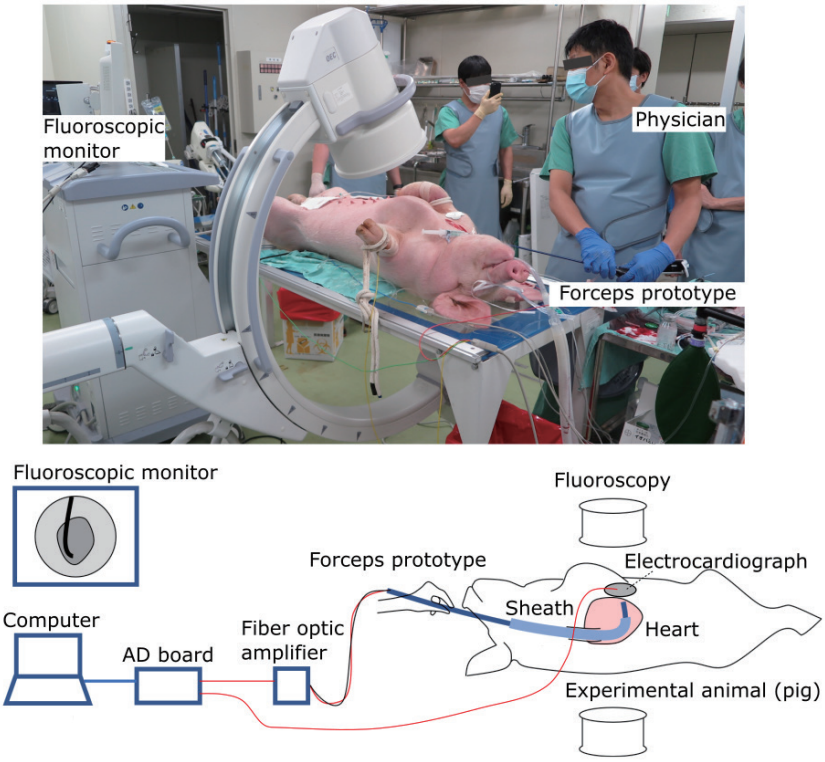

Fig. 16. (Color online) Setup of animal experiment.

3. Results

3.1 *In vitro* experiment: change of light amount with respect to vertical external force

The experimental results of the 3 mm forceps model are shown in Figs. 17 and 18. Figure 17 is time-series data. The values of optical fiber sensors A, B, and C are represented by the change rate of the reflected light on the left vertical axis, and the force measurement value of the force sensor is shown on the right vertical axis. Figure 18 shows the relationship between the measured vertical force and the change rate of the reflected light. In Fig. 17, the change rate of the reflected light of the three sensors showed almost the same curve. In Fig. 18, when the forceps tip was pushed, the change rate of the reflected light increased linearly until the measured force reached 1.4 N. This performance satisfies the target measurement range of 0–0.5 N described in Sect. 2.4. The target force detection range of 0–0.5 N was measured on the basis of the change rate of the reflected light of about 0–30% as shown in Fig. 18; therefore, the prototype will achieve our target specification (i), that is, binary judgment with and without contact is possible.

We assumed that the reason why the change rate in the reflected light did not change significantly even if the pushing force increased further was that the compression spring part of the shaft was in close contact and reached the end of the motion range when the force of 1.4 N was applied. In addition, the reason why the change rate of the reflected light differs between

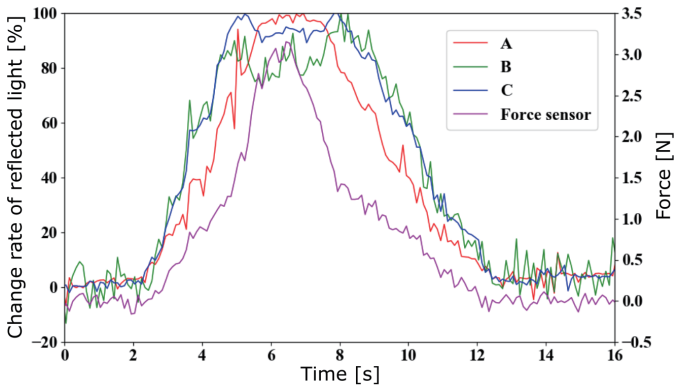

Fig. 17. (Color online) Time series data of reflected light and vertical force.

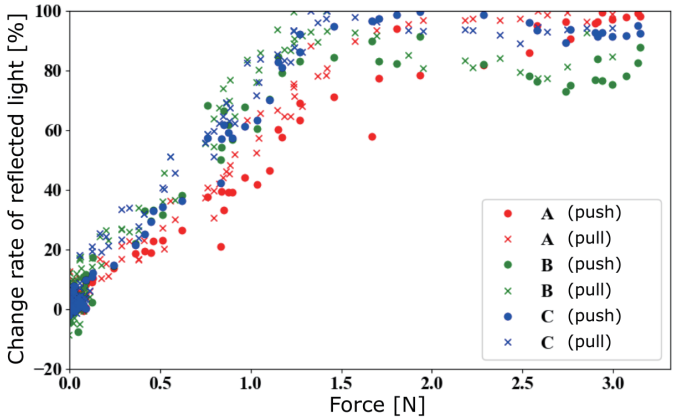

Fig. 18. (Color online) Relationship between vertical force and reflected light.

when the external force increases and when it decreases is assumed to be due to the hysteresis of the spring. From the results, we found that the amount of reflected light changed in proportion to the vertical external force until the spring reached the close contact state, and we confirmed that the external force in the vertical direction can be detected by the proposed prototype.

3.2 *In vitro* experiment: change of light amount with respect to the bending angle

The experimental results of the 3 mm forceps model are shown in Figs. 19–21. The rotation angle is shown on the horizontal axis, and the change rate of the reflected light is shown on the vertical axis. In the cases of 30 and 45 deg bending, the change rate of the reflected light showed almost the same outline for all sensors, and the angle values whose change rate became the maximum differed by 120 deg in each sensor. The transition region was within ±100 deg with respect to the rotation angle whose change rate of the reflected light was maximum, and the change rate was small in the other ranges. These measured trends seemed natural compared with the reflected light power calculation described in Sect. 2.3. There was no rotation angle at which the light change rates of all three sensors were equal. On the other hand, when the vertical force

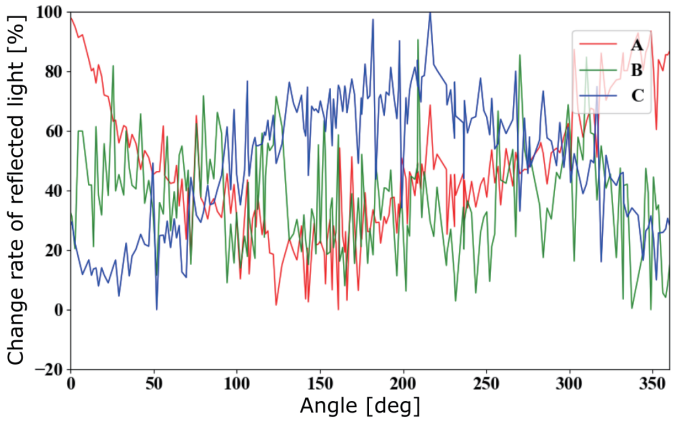

Fig. 19. (Color online) Relationship between rotation angle and reflected light (15 deg bending).

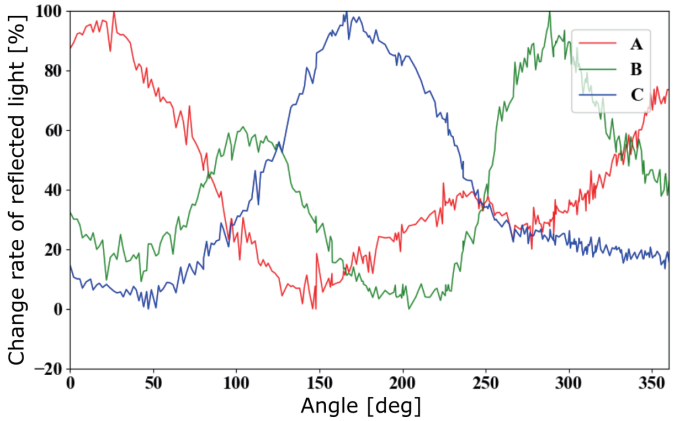

Fig. 20. (Color online) Relationship between rotation angle and reflected light (30 deg bending).

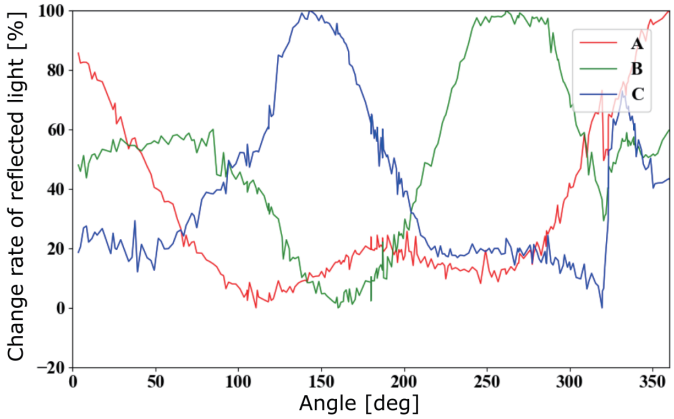

Fig. 21. (Color online) Relationship between rotation angle and reflected light (45 deg bending).

was applied as described in the previous section, all the sensors showed the same change rate of the reflected light. As a result, we confirmed that it is possible to detect the bending angle

change over 30 deg from the no-load state and the state with the vertical force. We confirmed that the proposed forceps model satisfied the target specification (ii), that is, the mechanism can judge whether there is a large bend or not.

In the cases of 30 and 45 deg bending, a first-order approximation of the transition region from 0 to 100% light amount for a 100 deg rotation gave a resolution of about 1%/deg. Regarding accuracy, the measured light amount contained white noise of about ±10%. This noise level is sufficiently small compared to 100% of the signal variation to enable binary bending mode judgment. Regarding measurement stability, the measurement of the proposed mechanism depends only on the relative positions between parts (geometric conditions) and external environmental conditions. Therefore, if there is no mechanical failure or environmental change during the measurement, highly reproducible results can be expected.

Note that there were some irregular changes as follows. In the case of 15 deg bending shown in Fig. 19, the sensors' signal-to-noise ratio was not good compared with the over 30 deg bending cases. A first-order approximation of the transition region from 20 to 80% light amount for a 100 deg rotation gave a resolution of about 0.6%/deg. Regarding accuracy, the measured light amount contained white noise of about ±20%. This noise level is not negligible compared to 60% of the signal variation. When the bending angle was small, the reflected light power became weak considering Eq. (4), and the noise signal power caused by irregular reflection inside the coil spring shaft became relatively large. However, we consider that the small bending angle will not prevent the sampling task, and the proposed angle detection method will be effective in practical use.

In addition, for the sensor B of near 100 deg in Figs. 20 and 21, the change rate of the light became also large in the part other than the transition region near 280 deg. We assumed the problem to be due to the misalignment between the reflector and the fixing part. We consider the problem as not serious and can be solved by precise manufacturing.

From the above results, we confirmed that the conical reflector was effective for the bending angle detection over 30 deg. By using the conical reflector, the tip posture change can be detected even for the external force in the bending direction other than the vertical direction in the 3 mm model.

3.3 Results of animal experiment

The results of the animal experiment are shown in Fig. 22. These are time-series data of the optical fiber sensor and the electrocardiogram voltage. The values of the optical fiber sensors A, B, and C are shown on the left axis, and the values of the electrocardiogram voltage are on the right axis. The physician estimated the contact state of the forceps tip subjectively from the image on the fluoroscopic monitor, and we compared the physician's comment with the measured data. In the case of no contact, the fluctuation of the reflected light amount was small. We considered that at the time between 3.5 to 13.5 s (Fig. 22), the forceps tip was in contact with the myocardial wall. In the case of contact, the change rate of reflected light fluctuated in synchrony with the change in the electrocardiogram. The sensor C showed the most clearly synchronized change along with the electrocardiogram signal. The sensors A and B showed relatively small changes in the contact state but showed large changes at the time of initial

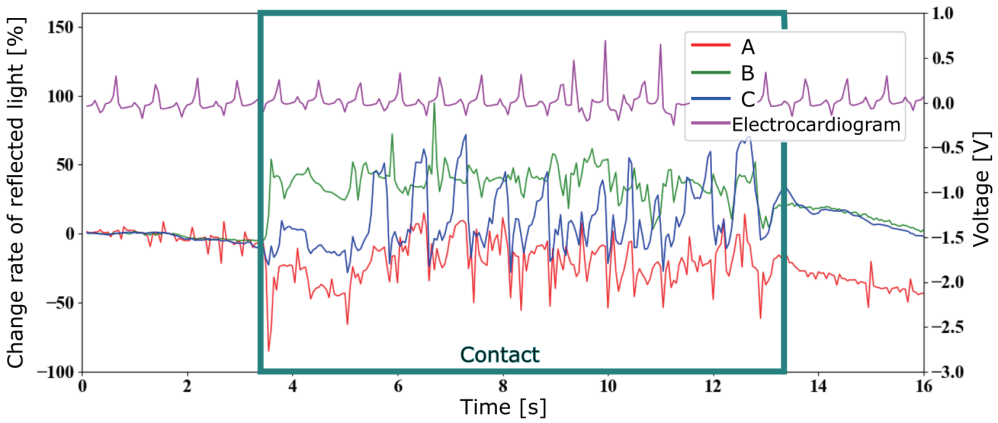

Fig. 22. (Color online) In vivo experiment results of optical fiber sensor forceps.

contact at 3.5 s. Using multiple sensor information will be useful for robust contact detection such as initial contact and fluctuation signal. We considered that the absolute amount of the reflected light of each sensor differs considerably depending on the bending direction, and the relative amount of influence differs depending on the sensor even with the same magnitude noise.

From the above results, we confirmed that the contact between the forceps tip and the myocardial wall can be detected in an *in vivo* environment using the proposed mechanism prototype.

4. Discussion

From our experimental results, we confirmed that the reflected light amount actually changed due to the deformation of the compression spring part that received the external force. With the prototype manufactured this time, it is possible to roughly judge the deformation state such as the no-load state, vertical compression state, and bending state. The main focus of this study was to propose and realize a detection mechanism that can be used *in vivo* and meets the specifications for binary mode judgement described in Sect. 2.1.2. On the other hand, resolution and accuracy, which are important indexes for continuous analog measurement, have room for improvement in the current handmade prototype. Since improving the resolution and accuracy is directly related to improving the detection performance of the proposed mechanism, we consider this task as one of our future works. When considering the practical application of the proposed mechanism in the future, the manufacturing process of the mechanism should be revised to reduce individual differences during mass production so that detection with higher accuracy and reproducibility is possible. For example, in this prototype, the compression spring part was created manually to simplify the manufacturing process. Since the manual process causes large individual differences, we will study a method for designing and manufacturing the mechanical properties of the compression spring part so that the performance is suitable for the myocardial biopsy task.

In addition, the proposed forceps prototype manufactured in this study has a simple mechanism without a jaw. As an experiment in the next stage, we will confirm whether the change of the reflected light due to the external force at the tip can be observed using the shaft deformation by the jaw opening and closing mechanism. Therefore, we plan to manufacture a prototype with the jaw mechanism in the future.

5. Conclusion

In this paper, we proposed and manufactured a novel contact force and bending angle detection mechanism using LIM-type optical fiber sensors for realizing an appropriate contact state in a myocardial biopsy task. We manufactured a prototype of the proposed forceps model and evaluated its characteristics through *in vitro* and *in vivo* experiments. In the *in vitro* experiments, we evaluated the relationship between the vertical or bending force on the forceps tip and the amount of the reflected light from the optical fiber sensor. In the case of the vertical force, we confirmed that the amount of the reflected light changed linearly in the range of the force under 1.4 N. In the case of the bending force, the light change curve with respect to the bending angle over 30 deg showed the same outline for all three pairs of sensors. We confirmed that the rotation angles at which the change rates of the reflected light become maximum differ by 120 deg for each sensor. Through these experiments, we confirmed that it is possible to detect the external force applied to the forceps tip in any direction. In addition, in the *in vivo* animal experiment, we confirmed that changes in the amount of light synchronized with the electrocardiogram. As the result, we confirmed the possibility of detecting the contact state between the forceps tip and the myocardial wall in an *in vivo* environment.

Acknowledgments

The authors would like to thank Katsuhiro Ohuchi of Tokyo Medical and Dental University and Norikatsu Okada and Yuuki Ootake of Technowood Corporation for their support. This research was supported by KAKENHI (20K08443).

References

1 S. Sakakibara and S. Konno: Jpn. Heart J. **3** (1962) 537. https://doi.org/10.1536/ihj.3.537
2 S. Konno and S. Sakakibara: Dis. Chest. **44** (1963) 345. https://doi.org/10.1378/chest.44.4.345
3 M. Sekiguchi, T. Nishikawa, M. Hiroe, and S. Morimoto: J. JCS Cardiologists **7** (1999) 363 (in Japanese). https://doi.org/10.1253/jjcsc.7.2_363
4 M. Holzmann, A. Nicko, U. Kühl, M. Noutsias, W. Poller, W. Hoffmann, A. Morguet, B. Witzenbichler, C. Tschöpe, H.-P. Schultheiss, and M. Pauschinger: Circulation **118** (2008) 1722. https://doi.org/10.1161/CIRCULATIONAHA.107.743427
5 O. Leone, J. P. Veinot, A. Angelini, U. T. Baandrup, C. Basso, G. Berry, P. Bruneval, M. Burke, J. Butany, F. Calabrese, G. d'Amati, W. D. Edwards, J. T. Fallon, M. C. Fishbein, P. J. Gallagher, M. K. Halushka, B. McManus, A. Pucci, E. R. Rodriguez, J. E. Saffitz, M. N. Sheppard, C. Steenbergen, J. R. Stone, C. Tan, G. Thiene, A. C. van der Wal, and G. L. Winters: Cardiovasc. Pathol. **21** (2012) 245. https://doi.org/10.1016/j.carpath.2011.10.001
6 L. T. Cooper, K. L. Baughman, A. M. Feldman, A. Frustaci, M. Jessup, U. Kuhl, G. N. Levine, J. Narula, R. C. Starling, J. Towbin, and R. Virmani: J. Am. Coll. Cardiol. **50** (2007) 1914. https://doi.org/10.1016/j.jacc.2007.09.008

7 T. Nishikawa, M. Sekiguchi, and H. Ishibashi-Ueda: Int. Heart J. **58** (2017) 840. https://doi.org/10.1536/ihj.16-316
8 R. Palmer: Gyn. Obst. **46** (1947) 420.
9 G. H. Ballantyne, P. F. Leahy, and I. M. Modlin: Br. J. Surg. **82** (1995) 140. https://doi.org/10.1002/bjs.1800820160
10 M. M. Scheinman, F. Morady, D. S. Hess, and R. Gonzalez: J. Am. Med. Assoc. **248** (1982) 851.
11 M. B. Mariano, M. V. Tefilli, T. M. Graziottin, C. M. P. Morales, and I. H. Goldraich: Eur. Urol. **49** (2006) 127. https://doi.org/10.1016/j.eururo.2005.09.018
12 D. O. Olsen: Amer. J. Surg. **161** (1991) 339. https://doi.org/10.1016/0002-9610(91)90592-2
13 G. Haber, S. Crouzet, and I. S. Gill: Eur. Urol. **54** (2008) 54. https://doi.org/10.1016/j.eururo.2008.03.076
14 E. Vaisbuch, C. Goldchmit, D. Ofer, A. Agmon, and Z. Hagay: Eur. J. Obstet. Gynecol. Reprod. Biol. **126** (2006) 234. https://doi.org/10.1016/j.ejogrb.2005.10.009
15 A. Finelli and I. S. Gill: Urol. Oncol. **22** (2004) 139. https://doi.org/10.1016/j.urolonc.2004.01.004
16 P. Puangmali, K. Althoefer, L. D. Seneviratne, D. Murphy, and P. Dasgupta: IEEE Sens. J. **8** (2008) 371. https://doi.org/10.1109/JSEN.2008.917481
17 S. Schostek, M. O. Schurr, and G. F. Buess: Med. Eng. Phys. **31** (2009) 887. https://doi.org/10.1016/j.medengphy.2009.06.003
18 A. L. Trejos, R. V. Patel, and M. D. Naish: Proc. Inst. Mech. Eng., Part C: J. Mech. Eng. Sci. **224** (2010) 1435. https://doi.org/10.1243/09544062JMES1917
19 G. F. Buess, M. O. Schurr, and S. C. Fischer: Arch. Surg. **135** (2000) 229. https://doi.org/10.1001/archsurg.135.2.229
20 U. Seibold, B. Kuebler, and G. Hirzinger: Proc. IEEE Int. Conf. Robot. Autom. (2005) 496. https://doi.org/10.1109/ROBOT.2005.1570167
21 J. Rosen, B. Hannaford, M. P. MacFarlane and M. N. Sinanan: IEEE Trans. Biomed. Eng. **46** (1999) 1212. https://doi.org/10.1109/10.790498
22 G. Tholey and J. P. Desai: Proc. IEEE Int. Conf. Robot. Autom. (2007) 250. https://doi.org/10.1109/ROBOT.2007.363795
23 K. J. Rebello: Proc. IEEE. **92** (2004) 43. https://doi.org/10.1109/JPROC.2003.820536
24 P. Valdastri, K. Harada, A. Menciassi, L. Beccai, C. Stefanini, M. Fujie, and P. Dario: IEEE Trans. Biomed. Eng. **53** (2006) 2397. https://doi.org/10.1109/TBME.2006.883618
25 M. Tanimoto, F. Arai, T. Fukuda, K. Itoigawa, M. Hashimoto, I. Takahashi, and M. Negoro: Medical Image Computing and Computer-Assisted Intervention – MICCAI 2000 (2000) 29. https://doi.org/10.1007/978-3-540-40899-4_4
26 N. Bandari, J. Dargahi, and M. Packirisamy: IEEE Access **8** (2020) 7682. https://doi.org/10.1109/ACCESS.2019.2962636
27 S. Nemoto and T. Makimoto: Opt. Quant. Electron. **11** (1979) 447. https://doi.org/10.1007/BF00619826
28 J. B. Faria: IEEE Trans. Instrumen. Meas. **47** (1998) 742. https://doi.org/10.1109/19.744340
29 P. Polygerinos, L. D. Seneviratne, and K. Althoefer: IEEE Trans. Instrumen. Meas. **60** (2011) 1408. https://doi.org/10.1109/TIM.2010.2085270
30 M. C. Yip, S. G. Yuen, and R. D. Howe: IEEE Trans. Biomed. Eng. **57** (2010) 1008. https://doi.org/10.1109/TBME.2009.2039570
31 P. Puangmali, H. Liu, L. D. Seneviratne, P. Dasgupta, and K. Althoefer: IEEE/ASME Trans. Mech. **17** (2012) 646. https://doi.org/10.1109/TMECH.2011.2116033
32 Y. Noh, H. Liu, S. Sareh, D. S. Chathuranga, H. Würdemann, K. Rhode, and K. Althoefer: IEEE Sens. J. **16** (2016) 7924. https://doi.org/10.1109/JSEN.2016.2600671
33 M. Tada, S. Sasaki, and T. Ogasawara: Sensors, 2002 IEEE (2002) 984. https://doi.org/10.1109/ICSENS.2002.1037244
34 H. Su and G. S. Fischer: in Proc. IEEE Int. Conf. Technologies for Practical Robot Applications (2009) 5. https://doi.org/10.1109/TEPRA.2009.5339654
35 P. Polygerinos, T. Schaeffter, L. Seneviratne, and K. Althoefer: Proc. Annual Int. Conf. IEEE Engineering in Medicine and Biology Society (2009) 1501. https://doi.org/10.1109/IEMBS.2009.5334163
36 S. B. Kesner and R. D. Howe: IEEE/ASME Trans. Mechatron. **16** (2011) 866. https://doi.org/10.1109/TMECH.2011.2160353
37 P. Polygerinos, L. D. Seneviratne, R. Razavi, T. Schaeffter, and K. Althoefer: IEEE/ASME Trans. Mechatron. **18** (2013) 386. https://doi.org/10.1109/TMECH.2011.2181405
38 R. Ahmadi, S. Arbatani, M. Packirisamy, and J. Dargahi: Biomed. Microdevices **17** (2015) 1. https://doi.org/10.1007/s10544-015-9931-3

39 I. B. Wanninayake: J. Phys.: Conference Series **1151** (2019) 012014. https://doi.org/10.1088/1742-6596/1151/1/012014
40 K. O. Hill, Y. Fujii, D. C. Johnson, and B. S. Kawasaki: Appl. Phys. Lett. **32** (1978) 647. https://doi.org/10.1063/1.89881
41 K. Yokoyama, H. Nakagawa, D. C. Shah, H. Lambert, G. Leo, N. Aeby, A. Ikeda, J. V. Pitha, T. Sharma, R. Lazzara, and W. M. Jackman: Circulation: Arrhythmia Electrophysiol. **1** (2008) 354. https://doi.org/10.1161/CIRCEP.108.803650
42 Y. L. Park, S. Elayaperumal, B. Daniel, S. C. Ryu, M. Shin, J. Savall, R. J. Black, B. Moslehi, and M. R. Cutkosky: IEEE ASME Trans. Mechatron. **15** (2010) 906. https://doi.org/10.1109/TMECH.2010.2080360
43 M. S. Müller, L. Hoffmann, T. C. Buck, and A. W. Koch: Int. J. Optomechatronics **3** (2009) 201. https://doi.org/10.1080/15599610903144146
44 S. Elayaperumal, J. H. Bae, B. L. Daniel, and M. R. Cutkosky: in Proc. IEEE/RSJ Int. Conf. Intelligent Robots and Systems. (2014) 3975. https://doi.org/10.1109/IROS.2014.6943121
45 T. Li, C. Shi, and H. Ren: IEEE/ASME Trans. Mechatron. **23** (2018) 2306. https://doi.org/10.1109/TMECH.2018.2856897
46 M. R. Islam, M. M. Ali, M.-H. Lai, K.-S. Lim, and H. Ahmad: Sensors **14** (2014) 7451. https://doi.org/10.3390/s140407451
47 W. Shang, H. Su, G. Li, C. Furlong, and G. S. Fischer: Sensors, 2013 IEEE (2013) 1. https://doi.org/10.1109/ICSENS.2013.6688137
48 H. Su, M. Zervas, G. A. Cole, C. Furlong, and G. S. Fischer: in Proc. IEEE Int. Conf. Robot. Autom. (2011) 1583. https://doi.org/10.1109/ICRA.2011.5979539
49 H. Su, M. Zervas, G. A H. Su, D. C. Cardona, W. Shang, A. Camilo, G. A. Cole, D. C. Rucker, R. J. Webster, and G. S. Fischer: Proc. IEEE Int. Conf. Robot. Autom. (2012) 1939. https://doi.org/10.1109/ICRA.2012.6224550
50 Z. Mo and W. Xu: IEEE Sens. J. **16** (2016) 8936. https://doi.org/10.1109/JSEN.2016.2619383
51 X. Liu, I. I. Iordachita, X. He, R. H. Taylor, and J. U. Kang: Biomed. Opt. Express **3** (2012) 1062. https://doi.org/10.1364/BOE.3.001062
52 Z. Mo, W. Xu, and N. Broderick: Proc. Int. Conf. Autom., Robot. Appl. (2015) 376. https://doi.org/10.1109/ICARA.2015.7081177
53 Y. Qiu, Y. Wang, Y. Xu, N. Chandra, J. Haorah, B. Hubbi, B. J. Pfister, and X. Liu: Biomed. Opt. Express **7** (2016) 688. https://doi.org/10.1364/BOE.7.000688
54 Y. Okumura, S. B. Johnson, T. J. Bunch, B. D. Henz, C. J. O'brien, and D. L. Packer: J. Cardiovasc. Electrophysiol. **19** (2008) 632. https://doi.org/10.1111/j.1540-8167.2008.01135.x
55 A. Hooshiar, S. Najarian, and J. Dargahi: IEEE Rev. Biomed. Eng. **13** (2020) 32. https://doi.org/10.1109/RBME.2019.2907458

About the Authors

Tomoyuki Umemoto received his Ph.D. degree in medicine from the Department of Cardiovascular Medicine, Tokyo Medical and Dental University, in 2017. From 2011 to 2015, he worked as a clinical fellow at Musashino Red Cross Hospital, Japan. He then worked as a clinical researcher at Mirano General Hospital, Italy. Since 2016, he has been an assistant professor at Tokyo Medical and Dental University, Japan. His research interests include cardiovascular medicine, biometric sensing technology, and medical device development. (umemoto.cvm@tmd.ac.jp)

Kei Sato received his master's degree from the Institute of Biomaterials and Bioengineering, Tokyo Medical and Dental University in 2021.
(k.s.nit.ac@gmail.com)

Tetsuro Miyazaki received his Ph.D. degree in engineering from the Department of Mechanical Sciences and Engineering, Tokyo Institute of Technology, in 2014. From 2014 to 2017, he worked as a research assistant (from 2014 to 2015) and an assistant professor (from 2015 to 2017) at Yokohama National University. From 2017 to 2020, he worked as an assistant professor at Tokyo Medical and Dental University. Since April 2020, he has been an assistant professor (from 2020 to 2021) and a lecturer (since January 2022) at the University of Tokyo. His research interests include mechanical engineering, control engineering, power assistive devices, and medical robotics. (Tetsuro_Miyazaki@ipc.i.u-tokyo.ac.jp)

Toshihiro Kawase received his B.S., M.S., and Ph.D. degrees from Tokyo Institute of Technology, Tokyo, Japan, in 2007, 2009, and 2012, respectively. He was a research fellow at the Research Institute of National Rehabilitation Center for Persons with Disabilities from 2012 to 2015 and a postdoctoral fellow and a specially appointed assistant professor at the Tokyo Institute of Technology from 2015 to 2017. From 2017 to 2022, he worked as an assistant professor at the Tokyo Medical and Dental University and Tokyo Institute of Technology. Since April 2022, he has been an associate professor at Tokyo Denki University. His research interests include medical robots, rehabilitation robotics, and biological signal processing. (tkawase@mail.dendai.ac.jp)

Maina Sogabe obtained a veterinary qualification in 2015 and received her Ph.D. degree in medicine from the Department of Medicine, Kyoto University, in 2020. From 2018 to 2020, she worked as a researcher on intravital imaging and microscopic data processing at Kyoto University. Since October 2020, she has been a researcher (from 2020 to 2022) and an assistant professor (since April 2022) at the Graduate School of Information Science and Technology of the University of Tokyo. Her research interests include biomedical data processing and analysis. (maina_sogabe@ipc.i.u-tokyo.ac.jp)

Tetsuo Sasano received his M.D. and Ph.D. degrees in medicine from Tokyo Medical and Dental University (TMDU) in 1993 and 2003, respectively. He started his career as a physician cardiologist and electrophysiologist. From 2003 to 2007, he worked as a postdoctoral fellow at Johns Hopkins University. He became an assistant professor in the Medical Research Institute of TMDU from 2007. From 2012 to 2019, he worked as an associate professor and has been a professor at TMDU since 2019. His interests are in basic and translational research to clarify the mechanism of arrhythmias and to develop novel diagnosis and treatment. He also works on applications of digital health including artificial intelligence.

Kenji Kawashima received his Ph.D. degree in engineering from the Department of Control Engineering, Tokyo Institute of Technology, in 1997. From 1997 to 2000, he worked as a research assistant at the Tokyo Metropolitan College of Industrial Technology. He then worked as an associate professor at the Precision and Intelligence Laboratory, Tokyo Institute of Technology. From 2013 to 2020, he worked as a professor at Tokyo Medical and Dental University. Since April 2020, he has been a professor at the University of Tokyo. His research interests include medical robotics, control engineering, and fluid measurement and control. (kkawa729@g.ecc.u-tokyo.ac.jp)